Another Look at the Refractive Index Structure Function*

T. CHERUBINI AND S. BUSINGER

University of Hawaii at Manoa, Honolulu, Hawaii

(Manuscript received 12 December 2011, in final form 3 August 2012)

ABSTRACT

This paper discusses the derivation of the refractive index structure function. It shows that the traditional formulation, which is based on the hydrostatic assumption, leads to increasing errors with height when compared with a formulation that is based on the potential temperature. The paper corrects a long-standing problem of extrapolating the traditional boundary layer approximation beyond its region of validity (i.e., to the upper troposphere and lower stratosphere). The new derivation may have applications in observational work to measure C_n^2 and seeing and in numerical modeling efforts. A preliminary analysis of the influence of the new formulation in numerical modeling of seeing suggests that impact on seeing will be small in general, because the largest contribution to seeing generally comes from the lower troposphere. However, an accurate C_n^2 profile is needed because other astroclimatic parameters, such as the isoplanatic angle, can suffer from the lack of C_n^2 accuracy at high altitude. This work may also have application in radar meteorology, since clear-air radar sensitivity depends on accurate estimation of C_n^2.

1. Introduction

The physical origin of the optical effects of atmospheric turbulence is in the random index-of-refraction fluctuations, also known as optical turbulence. The energy source for optical turbulence is derived from larger-scale wind shear or convection. Because an analytic solution of the equations of motion is not possible for turbulent flow, statistical treatments are used.

In general, turbulent flow in the atmosphere is neither homogeneous nor isotropic. However, it can be considered to be locally homogeneous and isotropic in small subregions of the atmosphere.[1] These regions are those whose scale lies between that of the larger eddies that make up the energy source for the turbulence and the small-scale eddies for which viscous effects become important. This region of locally isotropic turbulence is known as the inertial subrange (Fig. 1).

The fundamental statistical description of atmospheric turbulence in the inertial subrange was developed by Kolmogorov (1941) in terms of velocity field fluctuations. Kolmogorov assumed that the velocity fluctuations can be represented by a locally homogeneous and isotropic random field for scales smaller than the large eddies that provide the energy source for the turbulence. This implies that the second- and higher-order statistical moments of the turbulence depend only on the distance between any two points in the turbulent layer.

Using dimensional analysis, Kolmogorov showed that the structure function of the velocity field in the inertial subrange satisfies a universal $\frac{2}{3}$ power law. The turbulent fluctuations of the atmospheric refractive index n along the direction r are described by the refractive index structure $D_n(r)$. For locally isotropic turbulence fields, the structure function of the velocity field can be written as

$$D_n(\mathbf{r}) = \langle [n(\mathbf{x}) - n(\mathbf{x}+\mathbf{r})]^2 \rangle = C_n^2 r^{2/3}, \qquad (1)$$

where C_n^2 is called the refractive index structure coefficient and can be considered to be a measure of the strength of small-scale turbulence; here, angle brackets

[1] Local isotropy here refers to a particular part of the spectrum and not a geographic location.

* School of Ocean and Earth Science and Technology Contribution Number 8826 and Institute for Astronomy Preprint Number 13-005.

Corresponding author address: Dr. Tiziana Cherubini, Department of Meteorology, University of Hawaii at Manoa, 2525 Correa Rd., Honolulu, HI 96825.
E-mail: tiziana@hawaii.edu

DOI: 10.1175/JAMC-D-11-0263.1

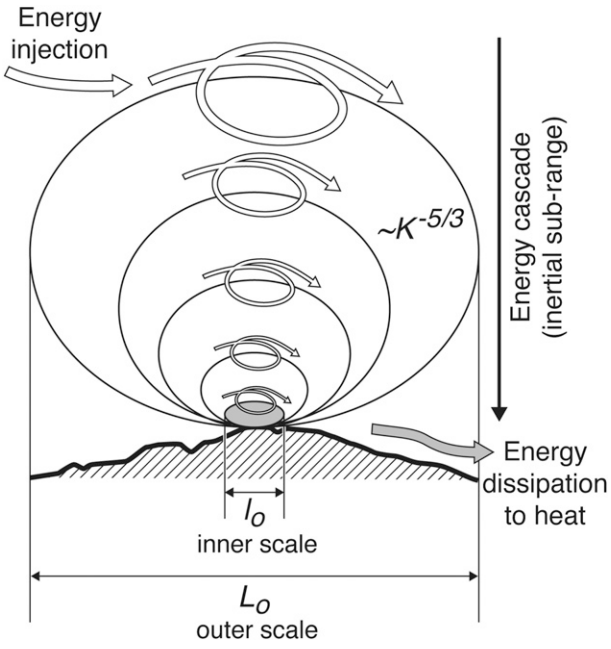

FIG. 1. Schematic illustration of the turbulent cascade process with the energy input region, inertial subrange, and energy dissipation region where energy is dissipated as heat. Here K is the spatial wavenumber and L is the eddy size (outer scale).

define the spatial average. In Kolmogorov's formulation $l \ll r \ll L$, with l being the inner scale, or the size below which viscous effects are important and energy is dissipated into heat, and L is the outer scale, or the size above which isotropic behavior is violated (Fig. 1). For eddies with sizes between the inner and outer scales, fluctuations in the refractive index are correlated. A detailed review of this formulation can be found in Tatarski (1961, 1971), Roddier (1981), and Vernin (2011). Astroparameters of importance for ground-based astronomy can be derived once C_n^2 is known (Roddier 1981; Businger and Cherubini 2011). Among these parameters, seeing is defined as

$$\varepsilon = 0.98\lambda/r_0, \tag{2}$$

where

$$r_0 = \left[0.423\left(\frac{2\pi}{\lambda}\right)^2 \int_0^{L_{\rm tp}} C_n^2(z)\, dz\right]^{-3/5} \tag{3}$$

is called the Fried number and $L_{\rm tp}$ is the total pathlength.

The isoplanatic angle (Roddier et al. 1982) is defined as

$$\vartheta_{\rm AO} = 0.057\lambda^{6/5}\left[\int_0^{\infty} z^{5/3} C_n^2(z)\, dz\right]^{-3/5}. \tag{4}$$

Fluctuations in the refractive index are related to corresponding fluctuations in temperature, pressure, and humidity. At high-altitude locations such as Mauna Kea, Hawaii, the humidity fluctuations in the infrared range of the spectrum account for less than 1% of the value of the index of refraction and pressure fluctuations are negligible. Therefore, the refractive index fluctuations associated with the visible and near-infrared region of the spectrum are caused primarily by random temperature fluctuations.

The statistical description of the random field of turbulence-induced fluctuations in the atmospheric refractive index is similar to that for the related velocity field fluctuations. The concept of a conservative passive additive (passive scalar) allowed Obukhov (1949) to relate the velocity structure function to the structure function for the variations on the refractive index C_n^2. In Tatarski (1961, 1971) C_n^2 is expressed as follows:

$$C_n^2(z) = a^2(K_H/K_M)L_0^{4/3}M^2, \tag{5}$$

where

$$M = -\frac{80\times10^{-6}p}{T^2}\left(\frac{\partial T}{\partial z}\right), \tag{6}$$

L_0 is the turbulent mixing length that characterizes the turbulent eddies, K_H and K_M are the exchange coefficients for heat and momentum, and a is an empirical constant.

The refractive index structure and the temperature structure, for most astronomical purposes, are related by (Roddier 1981)

$$C_n^2(z) = \left(\frac{80\times10^{-6}p}{T^2}\right)^2 C_T^2(z). \tag{7}$$

Tatarski (1961, 1971) pointed out that temperature is not a conservative passive additive and defines a pseudopotential temperature as

$$H = T + \gamma_a z, \tag{8}$$

which is an approximation of the potential temperature under conditions of hydrostatic equilibrium, where $\gamma_a = g/c_p$. He then derives an alternative formulation for M that takes into account the fact that in the free atmosphere (i.e., above the ground layer), the adiabatic lapse rate γ_a could be comparable to the environmental temperature gradient:

$$M = -\frac{80 \times 10^{-6} p}{T^2}\left(\frac{\partial T}{\partial z} + \gamma_a\right). \quad (9)$$

The derivation of (9) in Tatarski (1961, 1971) assumes that the atmosphere is in hydrostatic equilibrium and that the temperature change of a displaced parcel will follow an adiabatic lapse rate. Tatarski (1971) pointed out that this formulation is not valid for temperature fluctuations associated with larger vertical air motions. In Tatarski (1971), H is obtained by expanding θ in series and using the barometric equation, and this approximation is most valid in the lower troposphere.

Tatarski has referred to H as a ''potential temperature,'' which might have led to substitute θ for H in the structure function, and the following is found often in the literature:

$$C_n^2(z) = \left(\frac{80 \times 10^{-6} p}{T^2}\right)^2 C_\vartheta^2(z). \quad (10)$$

As a result there is a lack of clarity in the literature regarding the derivation of C_n^2 and what formulation of the refractive index structure function is best suited for which application. The goal of this note is to shed light on these issues. In particular, we demonstrate that application of Tatarski's formulation results in increasing errors aloft. These errors impact calculation of C_n^2 above the lower troposphere, and therefore the calculation of astroclimatic parameters like seeing and, more so, the isoplanatic angle. This latter one is in fact the integral of C_n^2 over the total optical path but weighted as $z^{5/3}$; therefore the upper profile is more important.

2. Another look at the refractive index structure function

Following Tatarski (1971), an analytical expression for C_n^2 is derived in this section from basic principles, using the potential temperature θ instead of H. For application with electromagnetic waves, the refractive index n can be expressed as follows:

$$n - 1 = \frac{80 \times 10^{-6}}{T}\left(p + \frac{4800e}{T}\right), \quad (11)$$

where T is temperature (K), p is pressure (hPa), and e is water vapor pressure (hPa). Because T and e are not conservative additives, (11) can best be expressed as a function of the potential temperature θ and the specific humidity q, which are both conservative variables. The potential temperature is defined as

$$\vartheta = T(p_0/p)^{R/C_v}, \quad (12)$$

where p_0 is the reference pressure at 1000 hPa, R is the ideal gas constant, and C_v is the heat capacity at constant volume. The specific humidity is defined by

$$e = 1.62pq. \quad (13)$$

Expression (11), in terms of θ and e, becomes

$$(n-1) \times 10^{-6} = N = \frac{80p}{\vartheta(p/p_0)^{R/C_v}}\left[p + \frac{4800 \times 1.62pq}{\vartheta(p/p_0)^{R/C_v}}\right]; \quad (14)$$

that is, $N = N[z, p(z), \theta(z), q(z)]$.

For example, suppose a parcel of air rises from height z_1 to z_2. The value of N for this parcel will undergo the following:

$$N_1 = N[z_1, p(z_1), \theta(z_1), q(z_1)] \rightarrow$$
$$N' = N[z_2, p(z_2), \theta(z_1), q(z_1)],$$

with θ and q conserving their values. Therefore the variation of the refractivity at level z_2 between the environment and the raised parcel is

$$\begin{aligned}\Delta N &= N[z_2, p(z_2), \vartheta(z_2), q(z_2)] \\ &\quad - N[z_2, p(z_2), \vartheta(z_1), q(z_1)] \\ &\approx \left(\frac{\partial N}{\partial \vartheta}\frac{d\vartheta}{dz} + \frac{\partial N}{\partial q}\frac{dq}{dz}\right)\Delta z. \end{aligned} \quad (15)$$

By applying (15) to (14) the following expression is found:

$$\frac{\Delta n}{\Delta z} = -\frac{80p}{\vartheta^2(p/p_0)^{R/C_v}}\left\{\left[1 + \frac{2 \times 4800 \times 1.62q}{\vartheta(p/p_0)^{R/C_v}}\right]\frac{d\vartheta}{dz} - \frac{(4800 \times 1.62)}{(p/p_0)^{R/C_v}}\frac{dq}{dz}\right\} \times 10^{-6}. \quad (16)$$

Using the potential temperature definition (16) becomes

$$M = \frac{\Delta n}{\Delta z} = -\frac{80 \times 10^{-6} p}{T\vartheta}\left[\left(1 + \frac{2 \times 4800 \times 1.62q}{T}\right)\frac{d\vartheta}{dz} - \frac{(4800 \times 1.62)}{T/\vartheta}\frac{dq}{dz}\right] \times 10^{-6}. \quad (17)$$

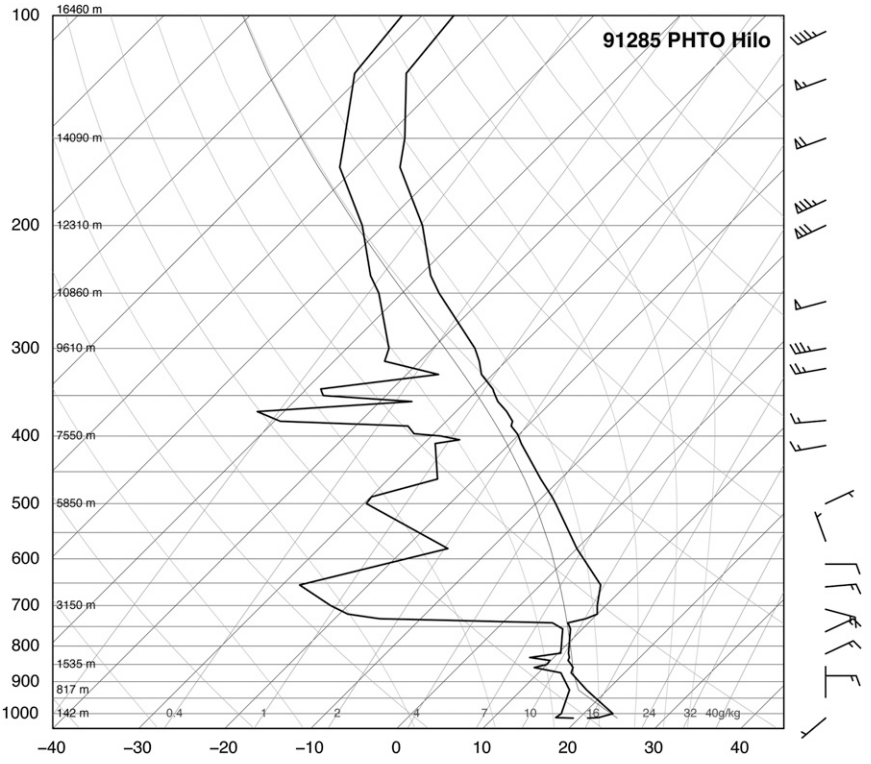

FIG. 2. Skew T diagram for Hilo, Hawaii, at 1200 UTC 23 Oct 2002.

Under conditions in which the contribution from moisture can be neglected, which is for most astronomical applications in the visible range, and following Tatarski's formalism, (17) becomes

$$M = -\frac{80\times10^{-6}p}{T\vartheta}\left(\frac{\partial\vartheta}{\partial z}\right). \tag{18}$$

This differs from (8) because of the presence in the denominator of the potential temperature and the use of potential temperature in the derivative and not the approximate form H. Accordingly, the expression for C_n^2 becomes

$$C_n^2(z) = \left(\frac{80\times10^{-6}p}{T\vartheta}\right)^2 C_\vartheta^2(z), \tag{19}$$

where

$$C_\vartheta^2(z) = a^2(K_H/K_M)L_0^{4/3}(\partial_\vartheta/\partial_z)^2. \tag{20}$$

Equation (19) provides the true constant structure function for the potential temperature. No approximations were needed in its derivation. The next two sections will show the difference between H and ϑ and the possible impact that using one versus the other might have in the estimation of optical turbulence.

Evaluating the difference between H and ϑ

A sample plot of H and ϑ as a function of height shows that H is a good approximation for ϑ for most of the atmosphere at and below the temperature inversion (Figs. 2, 3), where the difference between the two curves is at most 1°–1.5°C. However, the values of H and ϑ start to differ significantly at about 6–7 km above sea level; consequently their derivatives will also differ.

Current weather models that include algorithms to model optical turbulence extend well into the stratosphere. For these applications, ϑ is the better choice of conservative variable to use in these algorithms. The results from a case study of the impact of using one formulation versus the other in model calculations are presented in the next section.

3. Numerical model application of the new formulation

The model used in this study is the Weather Research and Forecasting (WRF) model (Klemp et al. 2007;

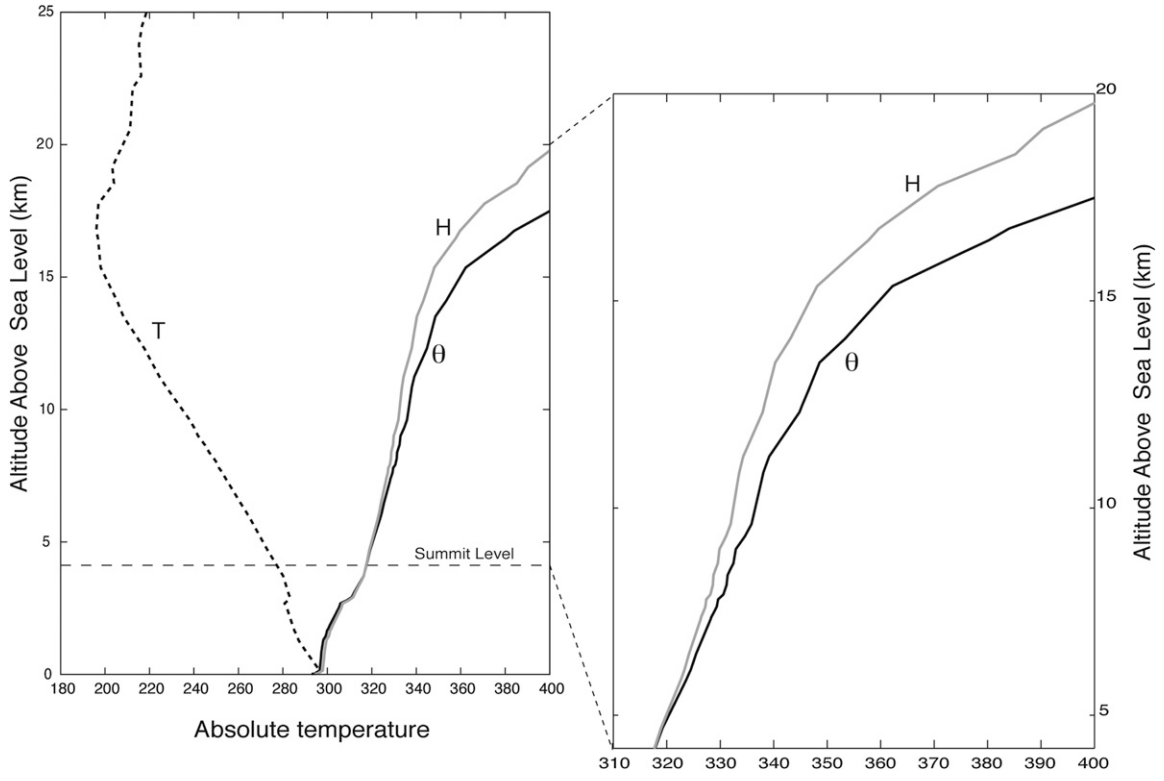

FIG. 3. (left) Temperature (short-dashed line), potential temperature (black line), and pseudopotential temperature as defined in Eq. (11) (gray line) calculated from the Hilo sounding at 1200 UTC 23 Oct 2002. For reference the long-dashed line indicates Mauna Kea's summit level. (right) More detail from the summit altitude to 20 km above sea level.

http://www.wrf-model.org). The model configuration chosen for this case study is the same operational configuration used at the Mauna Kea Weather Center (MKWC; http://mkwc.ifa.hawaii.edu; Businger et al. 2002). The configuration of WRF is the same as detailed in Cherubini et al. (2011), and the nested domains are shown in Fig. 4. The WRF model is initialized with the National Centers for Environmental Prediction Global Forecasting System (GFS) analyses. Boundary conditions are updated every 6 h also using the GFS analyses.[2]

In this implementation, the optical turbulence algorithm is parameterized following (18)–(20). The exchange coefficients for heat and momentum, K_H and K_M, are parameterized within the model planetary boundary layer scheme [Mellor–Yamada–Janjic scheme (MYJ); Janjic 2002], while the outer length scale of turbulence is parameterized as described in Masciadri et al. (1999). The full details regarding the optical turbulence algorithm are not included here for the sake of brevity and can be found in Cherubini et al. (2011).

In order for turbulent production to begin under conditions of a stable atmosphere, the turbulent scheme requires a nonzero background for the turbulent kinetic energy (TKE). Within the WRF MYJ boundary layer scheme, which solves the TKE budget equation, the background TKE is set to $E_{\min} = 0.1\ \mathrm{m^2\ s^{-2}}$. For optical turbulence purposes, however, this value is too large to produce realistic values of C_n^2 profiles in the upper troposphere. In this work the background TKE is set to $E_{\min} = 1 \times 10^{-4}\ \mathrm{m^2\ s^{-2}}$. Masciadri and Jabouille (2001) and Masciadri et al. (2004) proposed to calibrate the background TKE in the turbulent scheme. In the operational model setting, a calibration of $E_{\min}$ is included (see Cherubini et al. 2011). In this particular experiment, no calibration on $E_{\min}$ is performed since doing so is beyond the scope of this paper. Instead $E_{\min}$ is set as a constant with height: $E_{\min} = 1 \times 10^{-4}\ \mathrm{m^2\ s^{-2}}$.

Case study from the 2002 campaign

The vertical distribution of turbulence over Mauna Kea was measured as a part of a site characterization campaign held during October and December 2002.

[2] Using the GFS analyses instead of the GFS forecasts, as is usually done in an operational setting, helps to reduce the impact of forecast error.

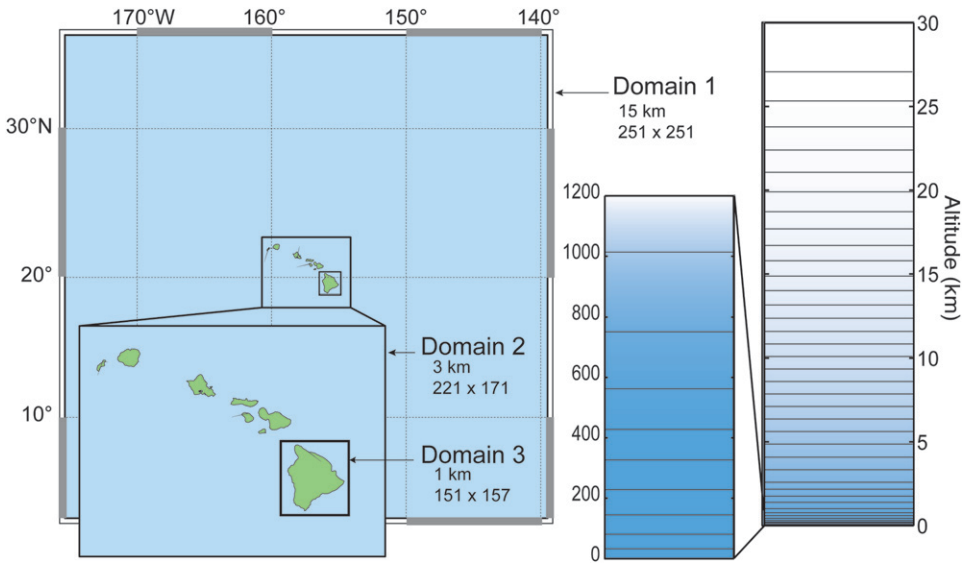

FIG. 4. MKWC configuration of the nested grids in WRF. Inset map shows an expanded view of the main island in the Hawaiian chain. (right) The vertical resolution of the model is depicted in the diagram, including an expansion of the lowest 1200 m of the model domain.

For the purpose of this work, only the data from the Generalized Scintillation Detection and Ranging (G-SCIDAR) for the October portion of the campaign are used. G-SCIDAR is an instrument that remotely measures the vertical distribution of the atmospheric turbulence by analyzing the stellar scintillation of a binary start target produced by the turbulent layers present in the atmosphere. For more details on the G-SCIDAR that was operated during the 2002 Mauna Kea campaign, the reader can refer to Cherubini et al. (2008).

Once the algorithm to calculate C_n^2 and seeing was revised in the WRF code as indicated in section 2, the model was rerun for 23 October 2002. WRF was initialized at 0000 UTC of that same nominal day. Optical turbulence profiles from the G-SCIDAR collected between 0600 UTC [2000 Hawaii–Aleutian standard time (HAST)] and 1600 UTC (0400 HAST) were considered and compared with the WRF output valid during the same timeframe. The C_n^2 simulated data are from the WRF innermost domain, with horizontal resolution of 1 km. Figure 5 shows the averaged nightly C_n^2 profiles for 23 October 2002, as observed and predicted by two WRF simulations, and illustrates the impact of the C_n^2 formulation, that is, whether (9) or (19) is used to calculate C_n^2. The comparison illustrates how, as expected, the differences among the C_n^2 profiles increase with height given the intrinsic differences between T and θ and given the differences, already described in section 3, between H and θ. This same experiment has been repeated for 22 and 24 October 2002, and the results show similar findings (not shown).

Clearly, the choice of the denominator in the C_n^2 definition has an appreciable impact on the simulated C_n^2 profiles. The two formulations of C_n^2 provide the same vertical profile shape but different inclinations/intensities. The analytical derivation in section 2, free of approximations, suggests that the correct formulation is provided by (18) and (19). No calibration is included in the results shown in Fig. 5, because a discussion of calibration is beyond the scope of this paper.

A seeing monitor was installed at the summit of Mauna Kea in September 2009. The seeing monitor is composed of two parts: a multiaperture scintillation sensor (MASS) and a differential image motion monitor (DIMM). MASS relies on the analysis of scintillation of single stars (Kornilov et al. 2003) and provides an integrated value of C_n^2 over each of six atmospheric layers. These layers are centered at 0.5-, 1-, 2-, 4-, 8-, and 16-km altitude above the site (Kornilov et al. 2003). MASS also provide the total free-atmosphere seeing. On the other hand, DIMM measures the integral of C_n^2 from the variance of the differential wave front tilts in two (or more) small apertures (Sarazin and Roddier 1990; Tokovinin 2002). The seeing monitor has been providing real-time data that are useful for C_n^2 algorithm verification purposes since its installation.

The optical turbulence algorithm implemented in the current version of the operational WRF model running at the MKWC includes these latest findings. Figure 6 shows an example of good agreement between the seeing observed by the seeing monitor and predicted seeing. In this particular case, the WRF algorithm was able to

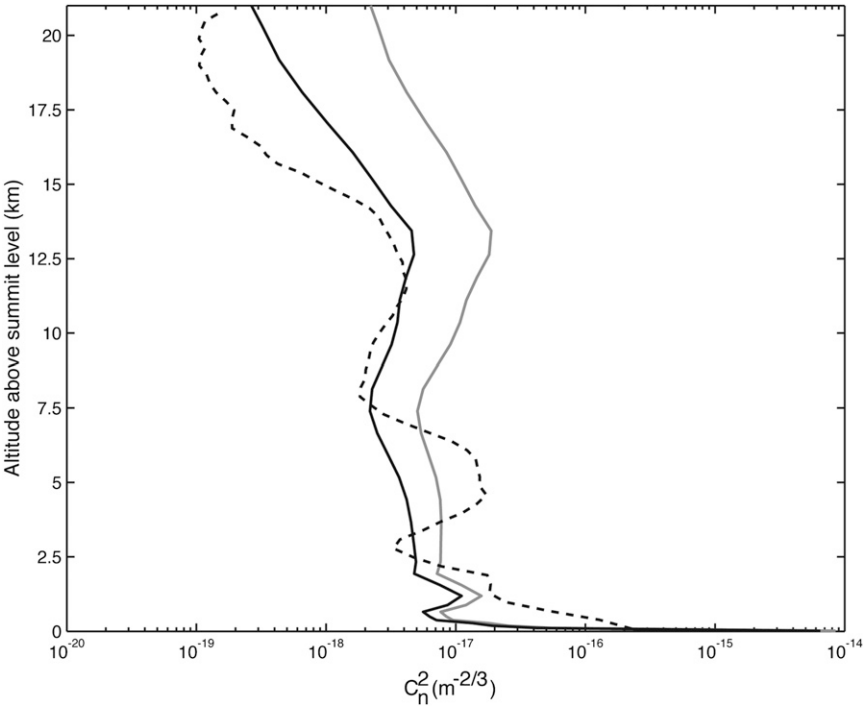

FIG. 5. Averaged nightly C_n^2 profile for 23 Oct 2002 as observed (black dashed line) and predicted by the WRF algorithm when T^2 (gray solid line) and θ (black solid line) are used, respectively, in the definition of C_n^2.

capture not only the average nightly seeing value but also the variability through the night. The value of this kind of graphic, which is produced operationally and posted on the MKWC Internet site, is that it allows the forecaster to quickly verify the performance of the seeing algorithm on a daily basis.

4. Conclusions and discussion

A review of the derivation of the refractive index structure function C_n^2 is provided in this paper to address a perceived lack of clarity in the literature regarding this topic. In this paper, C_n^2 has been derived following Tatarski (1961, 1971), but, unlike in Tatarski (1961, 1971), the potential temperature ϑ is used as the passive conservative variable instead of the pseudopotential temperature $H = T + \gamma_a$, which presumes that the atmosphere is in hydrostatic equilibrium. The difference between H and ϑ is illustrated through an example in section 3. Results from a sample case study show a positive impact for the upper troposphere when using the newer formulation of C_n^2 [(18)] versus the traditional formulation [(9)] in an optical turbulence algorithm implemented in the WRF model. The case study improved the agreement between observations and the synthetic C_n^2 profiles in the upper troposphere. The new formulation of C_n^2 may have applications in observational work to measure C_n^2 and seeing.

Moreover, other observational systems can benefit from a corrected formulation of C_n^2. For example, the clear-air radar sensitivity is proportional to C_n^2 (Hardy et al. 1966). Sharp inhomogeneities in the atmospheric refractive index can result in the backscatter of the radar power (Bragg phenomenon). The corrected C_n^2 derivation may improve estimates of the performance of these systems at higher altitude. In a similar manner, radar wind profiler networks and microwave links detect scatter from clear-air refractive index irregularities (Van Zandt et al. 1978; Van Zandt 2000; Marzano and D'Auria 1998). Although microwave applications need to account also for the water vapor, a corrected formulation of the C_n^2 that includes the use of potential temperature could improve the quantitative estimation of turbulence from these systems as well.

Work to construct a robust calibration of the revised optical turbulence algorithm is currently in progress. The use of data from the MASS–DIMM system, which has been operating at the summit of Mauna Kea since September 2009, and data from the Thirty Meter Telescope monitoring campaign will allow an accurate calibration that is based on data from a large sample of nights to more completely represent the range of turbulence

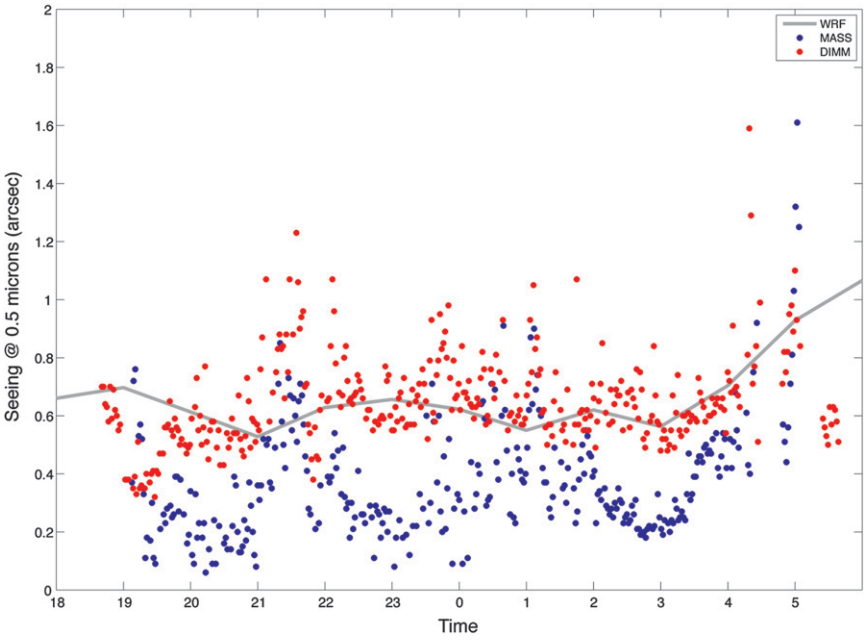

FIG. 6. Observed MASS (blue dots) and DIMM (red dots) seeing for the night from 1800 HAST 24 Oct 2011 to 0600 HAST 25 Oct 2011. The gray solid line is the WRF predicted seeing from the operational WRF run.

conditions associated with the naturally occurring atmospheric variability.

Acknowledgments. We thank René Racine for his constructive comments on an early draft. We also thank Elena Masciadri for insightful discussion on this subject and comments on an early draft.

REFERENCES

Businger, S., and T. Cherubini, Eds., 2011: *Seeing Clearly: The Impact of Atmospheric Turbulence on the Propagation of Extraterrestial Radiation.* VBW Publishing, 198 pp.

——, R. McLaren, R. Ogasawara, D. Simons, and R. J. Wainscoat, 2002: Starcasting. *Bull. Amer. Meteor. Soc.,* **83,** 858–871.

Cherubini, T., S. Businger, R. Lyman, and M. Chun, 2008: Modeling turbulence and seeing over Mauna Kea. *J. Appl. Meteor. Climatol.,* **47,** 1140–1155.

——, ——, and ——, 2011: An operational perspective for modeling optical turbulence. *Seeing Clearly: The Impact of Atmospheric Turbulence on the Propagation of Extraterrestrial Radiation,* S. Businger and T. Cherubini, Eds., VBW Publishing, 165–182.

Hardy, K. R., D. Atlas, and K. M. Glover, 1966: Multiwavelength backscatter from the clear atmosphere. *J. Geophys. Res.,* **71,** 1537–1552.

Janjic, Z. I., 2002: Nonsingular implementation of the Mellor-Yamada level 2.5 scheme in the NCEP Meso Model. NCEP Office Note 437, 61 pp.

Klemp, J. B., W. C. Skamarock, and J. Dudhia, 2007: Conservative split-explicit time integration methods for the compressible nonhydrostatic equations. *Mon. Wea. Rev.,* **135,** 2897–2913.

Kolmogorov, A. N., 1941: Local structure of turbulence in an incompressible viscous fluid at very large Reynolds numbers. *C. R. (Dokl.) Acad. Sci. URSS,* **30,** 301–305.

Kornilov, V., A. Tokovinin, O. Voziakova, A. Zaitsev, N. Shatsky, F. Potanin, and M. S. Sarazin, 2003: Mass: A monitor of the vertical turbulence distribution. *Adaptive Optical System Technologies II,* P. L. Wizinowich and D. Bonaccini, Eds., International Society for Optical Engineering (SPIE Proceedings, Vol. 4839), 837–845.

Marzano, F. S., and G. D'Auria, 1998: Model-based prediction of amplitude scintillation variance due to clear-air tropospheric turbulence on earth-satellite microwave links. *IEEE Trans. Antennas Propag.,* **46,** 1506–1517.

Masciadri, E., and J. P. Jabouille, 2001: Improvements in the optical turbulence parameterization for 3D simulations in a region around a telescope. *Astron. Astrophys.,* **376,** 727–734.

——, J. Vernin, and P. Bougeault, 1999: 3D mapping of optical turbulence using an atmospheric numerical model. I: A useful tool for the ground-based astronomy. *Astron. Astrophys. Suppl. Ser.,* **137,** 185–202.

——, R. Avila, and L. Sánchez, 2004: Statistic reliability of the Meso-NH atmospherical model for 3D C_n^2 simulations. *Rev. Mex. Astron. Astrofis.,* **40,** 3–14.

Obukhov, A. M., 1949: Structure of the temperature field in a turbulent flow (in Russian). *Izv. Akad. Nauk Arm. SSR, Geogr. Geofiz.,* **13,** 58–69.

Roddier, F., 1981: The effect of atmospheric turbulence in optical astronomy. *Prog. Opt.,* **19,** 281–377.

——, J. M. Gilli, and G. Lund, 1982: On the origin of speckle boiling and its effects in stellar speckle interferometry. *J. Opt.,* **13,** 263–271.

Sarazin, F., and F. Roddier, 1990: The ESO differential image motion monitor. *Astron. Astrophys.,* **227,** 294–300.

Tatarski, V. I., 1961: *Wave Propagation in a Turbulent Medium.* McGraw-Hill, 285 pp.

——, 1971: *The Effects of the Turbulent Atmosphere on Wave Propagation.* Israel Program for Scientific Translations, 482 pp.

Tokovinin, A., 2002: From differential image motion to seeing. *Publ. Astron. Soc. Pac.,* **114,** 1156–1166.

Van Zandt, T. E., 2000: A brief history of the development of wind-profiling or MST radars. *Ann. Geophys.,* **18,** 740–749.

——, J. L. Green, K. S. Gage, and W. L. Clark, 1978: Vertical profiles of refractivity turbulence structure constant: Comparison of observations by the sunset radar with a new theoretical model. *Radio Sci.,* **13,** 819–829.

Vernin, J., 2011: Optical turbulence for astronomy. *Seeing Clearly: The Impact of Atmospheric Turbulence on the Propagation of Extraterrestrial Radiation,* S. Businger and T. Cherubini, Eds., VBW Publishing, 17–44.